

Communication

o-Methoxy Substituents in Spiro-OMeTAD for Efficient Inorganic-Organic Hybrid Perovskite Solar Cells

Nam Joong Jeon, Hag Geun Lee, Young Chan Kim,
Jangwon Seo, Jun Hong Noh, Jaemin Lee, and Sang Il Seok

J. Am. Chem. Soc., **Just Accepted Manuscript** • DOI: 10.1021/ja502824c • Publication Date (Web): 16 May 2014

Downloaded from <http://pubs.acs.org> on May 21, 2014

Just Accepted

“Just Accepted” manuscripts have been peer-reviewed and accepted for publication. They are posted online prior to technical editing, formatting for publication and author proofing. The American Chemical Society provides “Just Accepted” as a free service to the research community to expedite the dissemination of scientific material as soon as possible after acceptance. “Just Accepted” manuscripts appear in full in PDF format accompanied by an HTML abstract. “Just Accepted” manuscripts have been fully peer reviewed, but should not be considered the official version of record. They are accessible to all readers and citable by the Digital Object Identifier (DOI®). “Just Accepted” is an optional service offered to authors. Therefore, the “Just Accepted” Web site may not include all articles that will be published in the journal. After a manuscript is technically edited and formatted, it will be removed from the “Just Accepted” Web site and published as an ASAP article. Note that technical editing may introduce minor changes to the manuscript text and/or graphics which could affect content, and all legal disclaimers and ethical guidelines that apply to the journal pertain. ACS cannot be held responsible for errors or consequences arising from the use of information contained in these “Just Accepted” manuscripts.

o-Methoxy Substituents in Spiro-OMeTAD for Efficient Inorganic-Organic Hybrid Perovskite Solar Cells

Nam Joong Jeon,^{†,§} Hag Geun Lee,^{†,§} Young Chan Kim,[†] Jangwon Seo,[†] Jun Hong Noh,[†] Jaemin Lee,^{*,†} and Sang Il Seok^{*,†,‡}

[†]*Division of Advanced Materials, Korea Research Institute of Chemical Technology, 141 Gajeong-Ro, Yuseong-Gu, Daejeon 305-600, Republic of Korea*

[‡]*Department of Energy Science, Sungkyunkwan University, Suwon 440-746, Korea*

Supporting Information

ABSTRACT: Three spiro-OMeTAD derivatives have been synthesized and characterized by ¹H/¹³C-NMR, and mass spectrometry. The optical and electronic properties of the derivatives were modified by changing the position of the two *p*-methoxy (–OMe) substituents in each of the quadrants, followed by UV-Vis spectroscopy and cyclic voltammetry measurements. The derivatives were employed as hole-transporting materials (HTMs) and their performances were compared for the fabrication of mesoporous (mp)-TiO₂/CH₃NH₃PbI₃/HTMs/Au solar cells. Surprisingly, the cell performance was dependent on the position of the *p*-, *m*-, and *o*-OMe substituents. The *o*-OMe substituents showed highly improved performance by exhibiting a short-circuit current density (*J*_{sc}) of 21.2 mA/cm², an open-circuit voltage (*V*_{oc}) of 1.02 V, and a fill factor (FF) of 77.6 % under illumination of 1 sun (100 mW/cm²), which resulted in an overall power conversion efficiency (PCE) of 16.7 %, compared to PCE (~15%) of conventional *p*-OMe positions. The PCE (16.7 %) is the highest value reported for perovskite-based solar cells to date with spiro-OMeTAD.

Very recently, hybrid halide perovskites (e.g. methylammonium lead halide: CH₃NH₃PbX₃, where X corresponds to halogens) were introduced as promising light harvesters in solar cells.¹⁻⁵ Mesoporous (mp) TiO₂ or Al₂O₃ was used as the scaffold for perovskite absorbers in the perovskite-based solar cells with hole-transporting materials (HTMs). In these cells, excited carriers can be injected into hole and electron transporting material for collection at the electrodes and the perovskite itself can behave as an electron or hole transporter, depending on the scaffold used.^{1,3} Recently, planar heterojunctions of a bulk layer of perovskite acting as both the absorber and long range transporter of charged species has shown the highest efficiencies.⁶⁻⁸ Currently, most state-of-the-art perovskite-based devices utilize spiro-OMeTAD ((2,2',7,7'-tetrakis(*N,N*-di-*p*-methoxyphenylamine)–9,9'-spirobifluorene)) the as HTM in their structures,^{1,2,4-8} although other types of HTMs were reported by several groups.^{3,9,10} For example, Graetzel et al. reported a 15.0% power conversion efficiency (PCE) for *np*-TiO₂/CH₃NH₃PbI₃/spiro-OMeTAD/Au.⁵ Snaith et al.⁶ showed a maximum efficiency of 15.4% with a *V*_{oc} of 1.07 V and a *J*_{sc} of 21.5 mA cm⁻², based on the CH₃NH₃PbI_{3-x}Cl_x deposited as thin layers with spiro-OMeTAD as the hole conductor. Initially, spiro-OMeTAD was used as a solid hole conductor in dye-sensitized solar cells (DSSCs) and it gave 0.74% PCE under full sunlight.¹¹ The PCE was increased by the

addition of 4-*tert*-butyl pyridine (t-BP) and lithium bis(trifluoromethanesulfonyl) imide (LiTFSI) in spiro-OMeTAD, which resulted in an enhanced PCE of 2.56% at one sun condition.¹² This system was further optimized and a PCE of 7.2% was reported by increasing the hole mobility of spiro-OMeTAD by more than one order of magnitude by doping it with a Co(III) complex and by using a high absorption coefficient organic dye.¹³

Several attempts were made to develop alternative organic HTMs for sensitized solar cells. Recently, we successfully developed an efficient inorganic-organic hybrid solar cell using poly(3-hexylthiophene) (P3HT) and poly[*N*-9-hepta-decanyl-2,7-carbazole-*al*-3,6-bis(thiophen-5-yl)-2,5-dioctyl-2,5-dihydropyrrolo[3,4-]pyrrole-1,4-dione] (PCBTDP) as effective hole conductors and Sb₂S₃ or Sb₂Se₃ as sensitizers.¹⁴⁻¹⁶ Thus, P3HT, PCPDTBT and poly-triarylamine (PTAA) were employed for the fabrication of hybrid halide perovskite solar cells.⁵ However, most of the HTMs are made of polymers whose synthesis and purification is difficult, with the possible disadvantage of incomplete filling of the mesoporous TiO₂ with spiro-OMeTAD. Small molecular HTMs such as *N,N'*-dialkyl perylene diimide (PDI) and *N,N'*-bis(3-methylphenyl)-*N,N'*-diphenylbenzidine (TPD) were also tried to increase the open circuit voltage of perovskite solar cells.¹⁰ Recently, we synthesized pyrene arylamine derivatives and applied them as HTMs in perovskite-based solar cells, but their performance was still poor when compared to spiro-OMeTAD.¹⁷

From the perspective of material's chemical structure, it is noteworthy that methoxy groups (–OCH₃; –OMe) were introduced to spiro-OMeTAD in order to control the oxidation potential of the materials. The –OMe group is electron withdrawing by inductive effect, but it can also exhibit electron-donating behavior under resonance stabilization. Depending on the substitution position, Hammett has reported two opposite effects of the –OMe substituent in the aromatic ring i.e., electron-donating for para (*p*) and electron-withdrawing for meta (*m*).¹⁸ In addition to such electronic effects, substitution at the ortho (*o*) position can also influence the oxidation potential by steric effect. Therefore, a simple and effective strategy to fine-tune the electronic properties is to change the substitution position of the –OMe group in arylamine-based HTMs. There are no reports on the application of *o*-, *m*-derivatives in spiro-OMeTAD as HTMs in perovskite-based solar cells. Hence, we decided to investigate the effect of replacing *p*- with *o*- and *m*- derivatives (see supplementary Figure S1 for the molecular structures) in spiro-OMeTAD.

In this study, we systematically changed the position of *p*-OMe substituents of spiro-type arylamine HTMs from *p* to *m* and *o*, and investigated their structure–property relationship in perovskite-based hybrid solar cells. Thus, we report the synthesis and characterization of three spiro-OMeTAD derivatives and their application in perovskite-based solar cells. The position of one of the two *p*-OMe substituents in each of the quadrants of spiro-OMeTAD was replaced with *m*- and *o*-OMe. The role of the *p*-OMe group in the spiro-OMeTAD substituent is to adjust the electronic properties of the hole conductor. Surprisingly, the cell using *o*-derivative in spiro-OMeTAD showed better performance compared to *p*- and *m*-derivatives with 16.7% overall power conversion efficiency (PCE) under AM 1.5G illumination at 100 mW/cm²; this is one of the highest PCE values reported to date for mp-TiO₂/CH₃NH₃PbI₃ perovskite/spiro-OMeTAD.

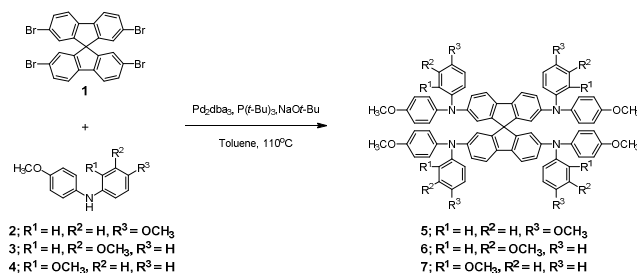


Figure 1. Synthetic routes for spiro-OMeTAD derivatives.

The procedures for the synthesis of the spiro-OMeTAD derivatives are shown in Figure 1 and experimental details are explained in the supporting information (SI). Spiro-OMeTAD derivatives were synthesized by the Buchwald–Hartwig amination reaction between 2,2',7,7'-tetrabromo-9,9'-spirobifluorene (**1**) and the respective dimethoxydiphenylamines containing *p*-OMe, *m*-OMe or *o*-OMe substituents (**2**, **3** and **4**, respectively). Compound **5**, which contains two *p*-OMe substituents in each of the quadrants, is the well-known spiro-OMeTAD, and in order to clearly define the substitution position, it is denoted as *pp*-spiro-OMeTAD in this study. The other two spiro-type arylamine derivatives with different substitution positions are denoted as *pm*-spiro-OMeTAD (**6**) and *po*-spiro-OMeTAD (**7**). All the three spiro-OMeTAD compounds were purified by column chromatography followed by recrystallization. They were characterized by ¹H/¹³C NMR spectroscopy, and mass spectrometry (see the Supporting Information). All the analytical data were consistent with the proposed structures. The three compounds have good solubility in all the common organic solvents.

The UV/vis absorption spectra of the three spiro-OMeTAD derivatives in the film state are shown in Figure 2a. All the derivatives showed absorption bands in the UV region, and the absorption maxima of *pp*-, *pm*-, and *po*-spiro-OMeTAD are centered at 387, 387, and 381 nm, respectively. The absorption onset wavelength that reflects the optical band-gap energy of the material helps in identifying the influence of the substitution position. The absorption onset of the three derivatives moved to shorter wavelength from *pp*- (423 nm) to *pm*- (413 nm), and further to *po*-spiro-OMeTAD (409 nm), which implies that the newly synthesized *pm*- and *po*-spiro-OMeTAD have increased band-gap energies compared to the well-known *pp*-spiro-OMeTAD.

In order to study the electrical properties of these compounds, we investigated the electrochemical properties by cyclic voltammetry (CV). As shown in Figure 2b, all the three compounds showed similar cyclic voltammograms in the oxidation scan.¹⁹ The first two overlapped oxidation peaks can be attributed to the two consecutive oxidation reactions of the molecule to generate a monocation radical and a quinoidal dication, respectively.²⁰ Inter-

estingly, the change of substitution position from *p*-OMe to *m*-OMe resulted in an increased oxidation potential. This is because the *m*-OMe group exerts an electron-withdrawing effect while the *p*-OMe group exerts an electron-donating effect, as previously reported by Hammett.¹⁸ However, contrary to *m*-substitution, substitution of the *p*-OMe group at the *o*-position did not show noticeable changes in the oxidation potential, which means that the electron-donating property of the *p*-OMe group is maintained in *o*-substitution. Based on the reported highest occupied molecular orbital (HOMO) energy level values (5.22 eV) of *pp*-spiro-OMeTAD,² HOMO energy levels of *pm*- and *po*-spiro-OMeTAD were calculated to be -5.31 and -5.22 eV, respectively.

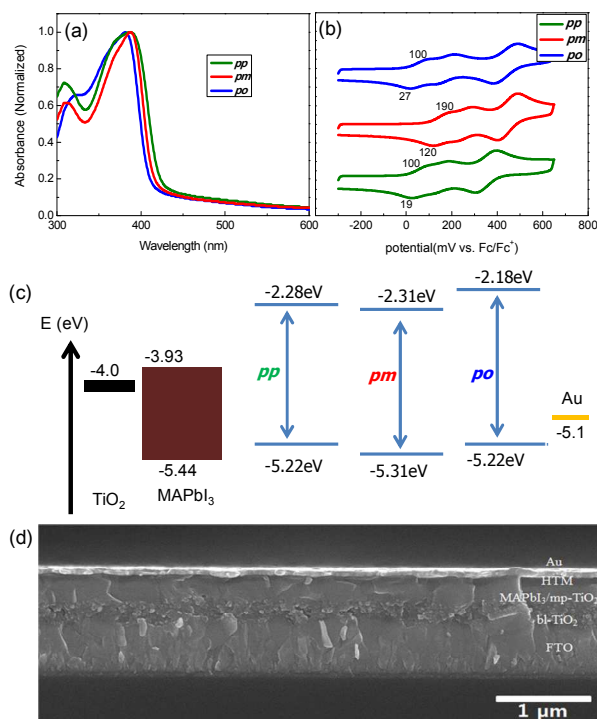


Figure 2. (a) UV/Vis absorption spectra of *pp*-, *pm*-, and *po*-spiro-OMeTAD in chlorobenzene. (b) Cyclic voltammograms of *pp*-, *pm*-, and *po*-spiro-OMeTAD. (c) Energy level diagram of the corresponding materials used in our devices. (d) Cross-sectional structure of the representative device.

Figure 2c shows the energy level diagram of the three spiro derivatives. The lowest unoccupied molecular orbital (LUMO) energy levels were calculated by adding the optical band-gap energies to the HOMO energy levels. The electronic effects of the spiro derivatives are observed to change substantially depending on the substitution position. Compared to the *p*-OMe, the *m*-OMe primarily decreased the HOMO energy level (ca. 0.09 eV). This is mainly due to the electron-withdrawing effect of the *m*-OMe substitution that does not contribute to resonance stabilization. On the other hand, the *o*-OMe increased the LUMO energy level (ca. 0.10 eV), compared to *p*-OMe mainly due to steric effect, i.e., the band-gap energy increased conceivably because of increased dihedral angle between the *o*-OMe-phenyl group and the fluorene ring, which results in a decrease of the effective conjugation of the molecule. The electron-donating effect of *o*- and *p*-OMe was almost the same as revealed by CV measurements.

We compared the similarities and differences in photovoltaic performance of the three spiro-OMeTAD derivatives as HTMs by fabricating the perovskite-based solar cells. For cell fabrication, we used a solvent mixture of γ -butyrolactone and dimethyl sul-

foxide to deposit a uniform $\text{CH}_3\text{NH}_3\text{PbI}_3$ (=MAPbI₃) layer.²¹ The cell was fabricated by spin coating a layer of MAPbI₃ onto the mp-TiO₂ surface, followed by drying at 100 °C. Spin coating of the *pp*-, *pm*-, and *po*-spiro-OMeTAD as HTMs was accomplished with Li-bis(trifluoromethanesulfonyl)imide (Li-TFSI), and 4-*tert*-butyl pyridine (*t*-BP) dissolved in toluene. In this study, we did not incorporate hole dopants like tris[2-(1H-pyrazol-1-yl)-4-*tert*-butylpyridine]cobalt(III) tris(bis(trifluoromethylsulfonyl)imide)] (FK209) because we can fabricate the cells with a very thin layer of spiro-OMeTAD. The same concentration of spiro-OMeTAD derivatives/toluene solutions for HTMs were used to keep very similar thickness them as overlayer on the perovskite. Finally, Au electrode was deposited on the top by thermal evaporation to complete the solar cell structure. Figure 2d shows cross-sectional image of the representative solar cell device fabricated in this work, as observed by a scanning electron microscopy (SEM). As can be seen, the MAPbI₃ perovskite forms a thin capping layer of about 350 nm with full infiltration into ~250-nm-thick mp-TiO₂ and a spiro-OMeTAD overlayer (~70 nm). The thickness of The thicknesses of the *pp*, *pm*, and *po* overlayers were almost similar, as estimated by same molecular weight. The gold contact on top of this organic conductor is also observed. In Figure 2c, the band alignment in TiO₂, MAPbI₃, and spiro-OMeTAD derivatives can be observed. The band alignment is such that the exciton dissociation and charge transfer at the interface are energetically favorable with possible driving force for a hole transfer from the MAPbI₃ into the spiro-OMe derivatives. Therefore, free charge carriers (or excitons) generated from the MAPbI₃ layer can be extracted (or dissociated) by transferring an electron to the underlying mp-TiO₂ layer through hole transfer to the spiro-OMeTAD HTM. However, there was a large hysteresis and distortion in the *J-V* curves in the reverse (from the open circuit voltage (*V*_{oc}) to the short circuit current (*I*_{sc})) and forward (i.e. from *I*_{sc} to *V*_{oc}) modes under standard air-mass 1.5 global (AM 1.5G) illumination for the perovskite-based solar cells, especially when it is measured at relatively short delay times.²¹ Such hysteresis and discrepancy leads to over- or under-evaluated performance which induces a considerable error in measuring the cell efficiency. This is because reliable solar cell *J-V* measurements should exhibit coincident curves from the forward and reverse directions. Figure S2 shows the variation of energy conversion efficiency for representative solar cell (using *po*-spiro-OMeTAD as HTM), measured by forward and reverse scans with 10 mV voltage steps and a delay time of 100 ms. Serious hysteresis is observed between both the scan directions with different performance; the efficiency in the reverse scan is 17.6%, while it is 14.1% in the forward scan. The efficiency measured by both the scan directions decreases and increases symmetrically with increasing delay time and then matched at 1000 ms, but average value remains almost the same after 300 ms (see supplemental Figure S3). Therefore, in this work, we showed current density-voltage (*J-V*) curves by averaging *J-V* curves obtained in both the scan directions with a delay time of 300 ms, because an excessively long measurement time is impractical.

With this in mind, we compared the photovoltaic performance of the cells fabricated using *pp*-, *pm*-, and *po*-spiro-OMeTAD derivatives. Figure 3a shows *J-V* curves for TiO₂/MAPbI₃/HTMs/Au solar cells fabricated using three HTMs and the photovoltaic parameters of these devices are summarized in Table 1. In all the cases, overlayer thickness of ~70 nm was observed in the SEM measurement (see Figure 2d). The device comprising of mp-TiO₂/MAPbI₃/*pp*-Spiro-OMeTAD gave an open-circuit voltage (*V*_{oc}) of 1.00 V, a short-circuit current density (*J*_{sc}) of 20.7 mA cm⁻², a fill factor (FF) of 71.1 %, and an overall conversion efficiency (η) of 14.9 %. These values are comparable and the cell performance is similar to that of the cells fabricated with commercial *pp*-spiro-OMeTAD (Merck), as reported by Gratzel et al.⁵ In contrast, the cells fabricated with *po*-spiro-

OMeTAD devices exhibit dramatically enhanced performance and the performance of cells fabricated from *pm*-spiro-OMeTAD is inferior to that of *pp*-spiro-OMeTAD. In Figure 3a, a small difference in *J*_{sc} and *V*_{oc} among *pp*-, *pm*-, and *po*-spiro-OMeTAD derivatives with a large difference in FF is observed. Generally, in solar cells, series resistance (*R*_s) reduces the FF, but does not affect *V*_{oc} and *J*_{sc}, if it is not excessively high values. A straightforward method of estimating the *R*_s from a solar cell is to find the slope of the *J-V* curve near the open-circuit voltage. As shown in the *R*_s determined from the slope of Table 1, *po*-spiro-OMeTAD-based cells showed lowest *R*_s of 32.96 Ω, whereas the *pp*- and *pm*-spiro-OMeTAD showed *R*_s of 45.37 Ω and 64.42 Ω, respectively. Besides *R*_s, the FF is also related to shunt resistance (*R*_{sh}). In perovskite-based solar cells consisting of mp-TiO₂-perovskite composite/perovskite layer/HTM/Au, the HTM functions as both hole-transporting and electron-blocking layer.³ *po*-spiro-OMeTAD having the highest LUMO will block electron flow into the metal electrode, which is responsible for increased *R*_{sh}. Therefore, *po*-spiro-OMeTAD effectively blocks the electron and transports the hole from MAPbI₃ to the Au electrode. Accordingly, the superior performance of *po*-spiro-OMeTAD may be rationalized in terms of the increased FF value through a low *R*_s and a high *R*_{sh}. However, further studies are needed to quantify the extent of this effect among *pp*-, *pm*-, and *po*-spiro-OMeTAD. Figure 3b shows monochromatic incident photon conversion efficiency (IPCE) spectrum for the cells fabricated using *pp*-, *pm*-, *po*- and commercial *pp*-spiro-OMeTAD, and the integrated photocurrent densities are in good agreement with the values measured in *J-V* curves, although the IPCE spectra differs slightly with wavelength.

Table 1. Average photovoltaic parameters for reverse and forward scanned-MAPbI₃ perovskite solar cells using commercial, *pm*-, *po*-, and *pp*-spiro-OMeTAD as HTMs

HTMs (spiro-OMeTAD)	<i>J</i> _{sc} (mA/cm ²)	<i>V</i> _{oc} (V)	FF	PCE (%)	<i>R</i> _s (ohm)
commercial-	20.4	1.00	73.7	15.2	37.35
<i>pm</i> -	21.1	1.01	65.2	13.9	64.42
<i>po</i> -	21.2	1.02	77.6	16.7	32.96
<i>pp</i> -	20.7	1.00	71.1	14.9	45.37

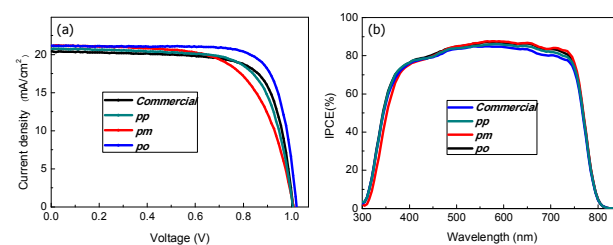


Figure 3. (a) Current density-voltage (*J-V*) curves for TiO₂/MAPbI₃/HTMs/Au fabricated with *pp*-, *pm*-, *po*- and commercial *pp*-spiro-OMeTAD as HTMs. (b) the corresponding IPCE spectra.

In summary, we synthesized *pp*-, *pm*- and *po*-spiro-OMeTAD derivatives that were applied as HTMs to the MAPbI₃ perovskite-based solar cells. Based on the CV measurements and UV-Vis spectra, the HOMO/LUMO energy levels of each derivative were characterized. The derivatives were used to fabricate feasible perovskite-based solar cells. Energy conversion efficiencies of 16.7% were obtained, which is the highest value reported till date

for perovskite-based solar cells with spiro-OMeTAD. The superior performance of *po*-spiro-OMeTAD was mainly attributed to the increased FF, owing to its low R_s and high R_{sh} . We believe that this study will open new avenues for the development of HTMs for perovskite-based solar cells for the fabrication of efficient and cost-effective photovoltaic devices.

ASSOCIATED CONTENT

Supporting Information

Details of experimental and additional supplementary figures. This material is available free of charge via the Internet at <http://pubs.acs.org>.

AUTHOR INFORMATION

Corresponding Author

* E-mail: seoksi@kriict.re.kr (seoksi@skku.edu) and jminlee@kriict.re.kr

Author Contributions

§ N.J.J. and H.G.L. contributed equally.

ACKNOWLEDGMENT

This work was supported by the Global Research Laboratory (GRL) Program, the Global Frontier R&D Program on Center for Multiscale Energy System funded by the National Research Foundation in Korea, and by a grant from the KRICT 2020 Program for Future Technology of the Korea Research Institute of Chemical Technology (KRICT), Republic of Korea.

REFERENCES

- (1) Lee, M. M.; Teuscher, J.; Miyasaka, T.; Murakami, T. N.; Snaith, H. *J. Science* **2012**, *338*, 643.
- (2) Kim, H.-S.; Lee, C.-R.; Im, J.-H.; Lee, K.-B.; Moehl, T.; Marchioro, A.; Moon, S.-J.; Humphry-Baker, R.; Yum, J.-H.; Moser, J. E.; Grätzel, M.; Park, N.-G. *Sci. Rep.* **2012**, *2*, 1.
- (3) Heo, J. H.; Im, S. H.; Noh, J. H.; Mandal, T. N.; Lim, C.-S.; Chang, J. A.; Lee, Y. H.; Kim, H.; Sarkar, A.; Nazeeruddin, M. K.; Grätzel, M.; Seok, S. I. *Nat. Photon.* **2013**, *7*, 486.
- (4) Noh, J. H.; Im, S. H.; Heo, J. H.; Mandal, T. N.; Seok, S. I. *Nano Lett.* **2013**, *13*, 1764–1769.
- (5) Burschka, J.; Pellet, N.; Moon, S.-J.; Humphry-Baker, R.; Gao, P.; Nazeeruddin, M. K.; Grätzel, M. *Nature* **2013**, *499*, 316.
- (6) Liu, M.; Johnston, M. B.; Snaith, H. J. *Nature* **2013**, *501*, 395.
- (7) Chen, Q.; Zhou, H.; Hong, Z.; Luo, S.; Duan, H.-S.; Wang, H.-H.; Liu, Y.; Li, G.; Yang, Y. *J. Am. Chem. Soc.* **2014**, *136*, 622.
- (8) Liu, D.; Kelly, T. L. *Nat. Photon.* **2014**, *8*, 133.
- (9) Giacomo, F. D.; Razza, S.; Matteocci, F.; D'Epifanio, A.; Licocchia, S.; Brown, T. M.; Carlo, A. D.; *J. Power Sources* **2014**, *251*, 152.
- (10) Edri, E.; Kirmayer, S.; Cahen D.; Hodes, G. *J. Phys. Chem. Lett.* **2013**, *4*, 897.
- (11) Bach, U.; Lupo, D.; Comte, P.; Moser, J. E.; Weissörtel, F.; Salbeck, J.; Spreitzer, H.; Grätzel, M. *Nature* **1998**, *395*, 583.
- (12) Krüger, J.; Plass, R.; Cevey, L.; Piccirelli, M.; Grätzel, M.; Bach, U. *Appl. Phys. Lett.* **2001**, *79*, 2085.
- (13) Burschka, J.; Dualeh, A.; Kessler, F.; Baranoff, E.; Cevey-Ha, N.-L.; Yi, C.; Nazeeruddin, M. K.; Grätzel, M. *J. Am. Chem. Soc.* **2011**, *133*, 18042.
- (14) Chang, J. A.; Im, S. H.; Lee, Y. H.; Kim, H.-J.; Lim, C.-S.; Heo, J. H.; Seok, S. I. *Nano Lett.* **2012**, *12*, 1863.
- (15) Choi, Y. C.; Mandal, T. N.; Yang, W. S.; Lee, Y. H.; Im, S. H.; Noh, J. H.; Seok, S. I. *Angew. Chem. Int. Ed.* **2014**, *53*, 1329.
- (16) Choi, Y. C.; Lee, D. U.; Noh, J. H.; Kim, E. K.; Seok, S. I. *Adv. Func. Mater.* DOI: 10.1002/adfm.201304238.
- (17) Jeon, N. J.; Lee, J.; Noh, J. H.; Nazeeruddin, M. K.; Grätzel, M.; Seok, S. I. *J. Am. Chem. Soc.* **2013**, *135*, 19087.
- (18) Hammett, L. P. *J. Am. Chem. Soc.* **1937**, *59*, 96.
- (19) Planells, M.; Abate, A.; Hollman, D. J.; Stranks, S. D.; Bharti, V.; Gaur, J.; Mohanty, D.; Chand, S.; Snaith, H. J.; Robertson, N. *J. Mater. Chem. A* **2013**, *1*, 6949.
- (20) Seo, E. T.; Nelson, R. F.; Fritsch, J. M.; Marcoux, L. S.; Leedy, D. W.; Adams, R. N. *J. Am. Chem. Soc.* **1966**, *88*, 3498.
- (21) Jeon, N. J.; Noh, J. H.; Kim, Y. C.; Yang, W. S.; Ryu S.; Seok, S. I. submitted.

TOC GRAPHICS.

